Orbital moment anisotropy of Pt/Co/AlO_{x} heterostructures with strong Rashba interaction

C. Nistor, T. Balashov, J. J. Kavich, A. Lodi Rizzini, B. Ballesteros, G. Gaudin, S. Auffret, B. Rodmacq, S.S. Dhesi, and P. Gambardella

Phys. Rev. B **84**, 054464 — Published 18 August 2011

DOI: 10.1103/PhysRevB.84.054464

Orbital moment anisotropy of Pt/Co/AlO_x heterostructures with strong Rashba interaction

C. Nistor,[1] T. Balashov,[1] J. J. Kavich,[1] A. Lodi Rizzini,[1] B. Ballesteros,[1] G. Gaudin,[2] S. Auffret,[2] B. Rodmacq,[2] S.S. Dhesi,[3] P. Gambardella[1,4,5]

[1] *Catalan Institute of Nanotechnology (ICN-CIN2), UAB Campus, 08193 Barcelona, Spain.*
[2] *SPINTEC, UMR-8191, CEA/CNRS/UJF-Grenoble 1/Grenoble-INP, INAC, F-38054 Grenoble, France.*
[3] *Diamond Light Source, Chilton, Didcot, Oxfordshire OX11 0DE, United Kingdom.*
[4] *Departament de Física, Universitat Autònoma de Barcelona, 08193 Barcelona, Spain.*
[5] *Institució Catalana de Recerca i Estudis Avançats (ICREA), 08100 Barcelona, Spain.*

PACS: 75.70.Tj, 75.30.Gw, 75.20.Hr, 78.70.Dm

Abstract: We study the anisotropy of the spin and orbital magnetization of ultrathin Co layers characterized by structure inversion asymmetry, namely Pt/Co/AlOx trilayers with Co thicknesses between 0.6 and 2 nm. We use x-ray magnetic circular dichroism (XMCD) to probe the Co layer along two orthogonal measurement geometries. By combining transverse and collinear XMCD, we achieve a vector measurement of the Co spin and orbital magnetic moments. We find an enhanced and anisotropic orbital magnetic moment localized at the Co interface and verify the connection between the Co orbital moment anisotropy and the macroscopic magnetic anisotropy of the trilayer. These results provide a link between diverse interfacial phenomena originating from spin-orbit coupling, such as the Rashba effect and perpendicular magnetic anisotropy. Using simple considerations derived from tight-binding models, we show that the Rashba constant is proportional to the ratio between out-of-plane and in-plane orbital magnetic moments.

I. Introduction

Ultrathin magnetic layers with surface-induced perpendicular magnetic anisotropy (PMA) are a dynamic field of research, owing to their applications in non-volatile high-density memory devices and intriguing theoretical implications. Following early predictions of interface-induced PMA by Néel [1] and subsequent confirmations in NiFe/Cu, Co/Pd, Co/Pt, Co/Au and Fe/Ag [2-6], a host of layered systems with surface-induced PMA has been proposed and studied [6-8]. New phenomena were discovered in these systems, such as enhanced spin and orbital magnetic moments [8-14]. It was demonstrated that PMA is driven by the orbital moment anisotropy, which couples the symmetry axes of the system to the spin magnetic moment [13,15-18]. Although the orbital magnetic moment contributes only with a small fraction (of the order of 10%) to the total magnetization, it simultaneously couples to the crystal field and to the spin magnetic moment (through spin-orbit coupling) and consequently mediates an interaction between the spin moment and the lattice. The anisotropy of the orbital moment was shown to occur either through hybridization of electronic states at a magnetic/non-magnetic metal interface or through interfacial strain.

Pt/Co/AlO_x trilayers exhibit strong PMA and have attracted considerable interest for applications in magnetic tunnel junctions (MTJ) with out-of-plane magnetization as well as in RF oscillators [19-22]. Pt/Co/AlO_x structures have the benefit of tunable PMA, which can be adjusted by controlling the oxidation time and annealing temperature [23]. Optimal oxidation and annealing conditions were shown to result in a smooth and fully oxidized Co/AlO_x interface with little O diffusion into the Co layer and strong PMA [23,24]. By using x-ray photoelectron spectroscopy (XPS) and x-ray absorption spectroscopy (XAS) it was shown that, in addition to Co/Pt hybridization, PMA in Pt/Co/AlO_x can be explained by interfacial Co oxidation [25]. The latter results

in a large density of interface Co-O bonds that favor the out-of-plane Co *d*-orbitals and polarize the Co/AlO_x interface [26].

Recently, we have found that the lack of structure inversion symmetry in Pt/Co/AlO_x trilayers induces a strong magnetization torque when an in-plane electric current flows in the Co layer [27]. This phenomenon is explained by the asymmetric stacking of Pt/Co and Co/AlO_x interfaces, which create a strong electric field inside the Co layer. In the conduction electron rest frame this electric field transforms into a magnetic (Rashba) field which couples, via s-d exchange interaction, to the Co layer magnetization [27-29]. The Rashba effect, together with PMA, makes Pt/Co/AlO_x trilayers attractive candidates for efficient spintronic devices. It shall be noted that the coexistence of strong PMA and the Rashba effect does not appear to be coincidental, as both are interfacial phenomena related to spin-orbit coupling. However, few studies of ferromagnetic systems displaying the Rashba effect have been performed [27,30], so that several outstanding questions remain open. In particular, the orbital moment anisotropy defining PMA might also be a necessary condition to achieve a strong Rashba interaction, since its origin lies in the large charge transfer (hybridization) perpendicular to the interface plane. Other questions, which will not be addressed here, concern the temperature dependence of the anisotropy and Rashba constants, as well as their optimization with respect to changes of the chemical composition of the interfaces.

In this article we perform an element-resolved vectorial measurement of the spin and orbital magnetic moments of Pt/Co/AlO_x trilayers as a function of Co thickness. The absolute magnetization values are affected by mild oxidation of the top Co interface. We find that the thinnest Co layer (0.6 nm) is characterized by the strongest orbital moment anisotropy. The thinner layers (0.6-1 nm) present PMA, whereas the thicker layers (1.5-2 nm) have in-plane easy axis. We verify the connection between

orbital moment anisotropy and magnetocrystalline anisotropy for Pt/Co/AlO_x, using models derived from perturbation theory [17,18] and fully-relativistic band structure calculations [15,31]. Finally, we discuss the relationship between the orbital moment anisotropy and the Rashba effect, showing that both PMA and the Rashba constants are expected to scale together.

II. Experiment

Four Pt(3 nm)/Co(t)/Al(1.6 nm) layered structures (t = 0.6, 1, 1.5, 2 nm) were deposited by conventional dc magnetron sputtering at room temperature onto thermally oxidized Si substrates. The deposition rates were 0.5 nm/s (Co and Al) and 1 nm/s (Pt) at an Ar pressure of $2x10^{-3}$ mbar (base pressure 10^{-8} mbar). After deposition the samples were oxidized by exposure to a radiofrequency (rf) oxygen plasma at a pressure of $3x10^{-3}$ mbar and an rf power of 10 W for 40 seconds. Non-annealed samples deposited following the above procedure were shown to be very stable over time and therefore no capping layer was needed [32].

In order to confirm the presence of the three layers, high-resolution transmission electron microscopy (HRTEM), scanning transmission electron microscopy (STEM) and energy dispersive x-ray spectroscopy (EDS) were performed on the samples. Specimens for electron microscopy were prepared in cross section geometry by mechanical grinding, dimpling, precision polishing and finally ion milling. HRTEM images and EDS-STEM spectra were recorded using a FEI Tecnai F30 equipped with an EDAX x-ray spectrometer and operated at 300 kV.

Fig. 1 displays HRTEM micrographs taken on specimens from the thinnest (a) and the thickest (b) Pt/Co/AlO_x trilayers. The analysis of the lattice spacings shows that the Pt buffer layer has a polycrystalline structure with the grains growing along the

(111) direction. The Co layer appears polycrystalline and rather uniform and homogeneous. Although for the Pt(3nm)/Co(0.6nm)/AlO_x sample there is not enough contrast to clearly discern between the Co and Pt layers in the HRTEM image, the presence of Co can be confirmed by EDS-STEM point analysis and line scans acquired in the same region. The composition profiles shown in (c) and (d) were derived from the quantification of the individual spectra of the EDS-STEM line scan, and for clarity the relative atomic percentages were calculated considering only the elements Al, Co, Pt and Si. Due to drift during the EDS-STEM acquisition, only the stacking sequence and elemental signatures can be inferred from the profiles but not the thickness and overlap of different layers.

XMCD measurements were performed on this series of samples in order to characterize their magnetic properties, particularly their spin and orbital magnetic moments. The XMCD technique consists in measuring the difference between absorption of right- and left-handed circularly polarized x-rays near a core absorption edge. In the case of Co, the spectra are taken by sweeping the x-ray photon energy across the L_3 and L_2 edges, which are the 2p→3d core-to-valence excitations. From these spectra one can extract the magnetic properties of the system through the XMCD sum rules [33,34]. If we define I_+ and I_- as the absorption intensities of right (+) and left (-) handed circularly polarized photons, then the projections of the orbital moment m_{ORB} and the spin moment m_{SPIN} of the absorbing element along the x-ray photon direction are given by:

$$(1)\quad \frac{m_{ORB}}{n_h} = -\frac{4\int_{L_3+L_2}(I_+ - I_-)dE}{3\int_{L_3+L_2}(I_+ + I_-)dE},$$

$$(2)\ \frac{m_{SPIN}^{eff}}{n_h} = \frac{m_{SPIN} + m_T}{n_h} = -\frac{6\int_{L_3}(I_+ - I_-)dE - 4\int_{L_3+L_2}(I_+ - I_-)dE}{\int_{L_3+L_2}(I_+ + I_-)dE},$$

where m_{ORB} and m_{SPIN} are expressed in μ_B/hole and n_h is the number of 3d holes above the Fermi level. I_+ and I_- are corrected by removal of contributions from transitions to the continuum, which is done by subtracting two step functions centered at the L_3 and L_2 edges with relative amplitudes of 2:1. The term m_T in sum rule (2) is the intra-atomic dipole moment, which can be decomposed into its diagonal components: $m_T = m_T^z \cos^2\theta + m_T^{xy} \sin^2\theta$ that satisfy the relation $m_T^z + 2m_T^{xy} = 0$ (θ is the angle between the photon direction and the sample normal). The dipole moment vanishes for a measurement performed at the ´magic angle´ $\theta \approx 55^0$ [35,36].

XMCD measurements were performed at I06 beamline of the Diamond Light Source, which supplies x-ray photons with 99±1% circular polarization. A superconducting magnet allowed the application of magnetic fields of up to 2 Tesla along any arbitrary direction. A 1.95 T field was applied to the sample in two distinct geometries, shown in Fig.2: the collinear geometry, with the field (H_z) applied parallel to the beam direction, and the transverse geometry, with the field (H_x) applied perpendicular to the beam direction. The transverse geometry was originally proposed as a method to measure the orbital and magnetic dipole moments, since in this geometry the spin moment contribution vanishes if the sample is fully saturated [15,36,37]. The x-ray absorption in the sample was monitored by measuring the total emitted photocurrent. In order to improve the signal-to-noise ratio and minimize artifacts in the measured photocurrent due to the large magnetic fields, averaged x-ray absorption spectra were recorded for all four combinations of photon helicities and magnetic field directions. The absorption spectra were normalized to the incident x-ray beam flux. All

measurements were performed at T = 200 K, the equilibrium temperature of the cryostat in the absence of active cooling or heating. These conditions were chosen in order to minimize electric interference from the heater in the measured signal. Because of saturation effects due to x-ray absorption in the sample, corrections have to be applied to the magnetic moment values obtained using the sum rules. For Co, it was shown that the saturation effects which occur in a 2 nm thick Co layer (the largest thickness in this experiment) consist in an underestimate of m_{ORB} and m_{SPIN} by up to ~ 10% and 5%, respectively [38]. These corrections (which scale approximately with the sample thickness) will be even smaller for the thinner Co layers, and will be neglected in our analysis.

III. Results

Prior studies have shown that the easy magnetization axis of Pt/Co/AlO_x depends on the thickness of the Co layer, with a transition from an out-of-plane easy axis at low Co thickness to an in-plane easy axis at larger Co thicknesses. This transition was attributed to the competition between interface anisotropy (which favors out-of-plane Co magnetization) and shape anisotropy (which favors in-plane Co magnetization). Depending on the preparation conditions, this critical thickness can take values in the range from 1 to 3 nm [21]. In order to find the easy magnetization axes in our samples, we measured out-of-plane hysteresis loops by recording x-ray absorption spectra as a function of field in collinear geometry at θ=0º. The hysteresis loops were plotted by taking the ratio R between the absorption at 777.7 eV (peak absorption at the L_3 edge) and the absorption at 770 eV (pre-edge absorption). It can be shown that R is approximately proportional to the Co layer magnetization M_{Co} [39], and we plot this ratio for the four samples in Fig.3. The Co(0.6 nm) and Co(1 nm) films have square

hysteresis loops that appear to saturate, which is evidence of an out-of-plane easy magnetization axis. On the other hand, the (minor) hysteresis loops of Co(1.5nm) and Co(2nm) films are non-hysteretic and consistent with an in-plane easy magnetization axis. Also note that both Co(0.6nm) and Co(1 nm) films are characterized by sharp magnetization reversals, which indicate that the Co films are uniform and continuous. This last assumption is also supported by the TEM micrographs in Fig.1.

A. XAS and XMCD in collinear and transverse geometry

XAS and XMCD spectra taken on the Co (0.6nm) and Co (2nm) samples at the Co $L_{2,3}$ edges are shown in Fig.4. These spectra contain information about the magnetic moments averaged over the thickness of the Co layers, due to the 2-3 nm typical escape depth of the photoelectrons excited by x-ray absorption. For each sample thickness, spectra were recorded in both collinear and transverse geometries at $\theta = 45^0$. The XAS spectra shown in Fig. 4 have the characteristic shape of a predominantly metallic Co layer [25]. A shoulder is visible on the L_3 edge peak (at ~781 eV) and is an indication of interfacial Co-O bonds. It was shown by surface-sensitive XPS measurements that exposure to oxygen plasma under optimal conditions (30-45s) oxidizes only the Co interface, with little oxidation of the bulk Co, however overexposure to the oxygen plasma allows diffusion of O into the Co layer (overoxidation) [25,40]. A comparison between our XAS spectra and previously reported spectra taken on similar Pt/Co(0.6nm)/AlOx samples suggests that our samples might be slightly overoxidized [40]. In the Co (0.6nm) film the ratio between the CoO and Co peaks in the derivative of the XAS spectrum (not shown) is about 2 times larger compared to the same ratio for the Co(2nm) film.

The collinear XMCD signal, shown in the left panels of Fig. 4, is substantially larger for Co(2nm) compared to Co(0.6nm), which, according to the second sum rule, results in a larger spin magnetic moment per Co atom in the thicker layer. In the transverse geometry, because the projection of the magnetization along the photon beam direction is close to zero, the XMCD is much smaller compared to the collinear case (Fig. 4, right panels). However, the transverse dichroism signal does not vanish for either sample, which shows that there is a non-vanishing value for either the transverse spin or the orbital moment, or both (contributions from m_T will be discussed in this section as well). Finally, we notice that the dichroism signal in transverse geometry has opposite signs for the two thicknesses, which we will show to be related to different angular orientations of the magnetic moments in the two samples.

Figure 5 shows XMCD spectra taken a) in the collinear geometry at $\theta = 0^\circ$ as a function of Co thickness and b) for different sample orientations and measurement geometries at fixed Co thickness (0.6 nm). All spectra were normalized to equal XMCD L_3 peak amplitudes. The lineshape of the XMCD spectra shows a clear trend as a function of both Co thickness and measurement geometry or sample orientation. In a), we notice that the L_2 peak amplitude decreases with decreasing thickness, which according to the first sum rule demonstrates an increasing orbital moment. In b), the lowest L_2 peak amplitude corresponds to the transverse geometry, as the XMCD spectral intensity is mostly of orbital origin in this case.

B. Co magnetization: XMCD sum rules results

In order to derive the spin moment values, we will need to first evaluate the magnetic dipole term m_T which appears in the second sum rule. If we define $\hat{e}$ as the

direction parallel to the sample normal, then for an arbitrary photon beam direction $\hat{P}$ the magnetic dipole term can be expressed as follows [36]:

(3) $m_T = \frac{1}{4} m_T^z \left[\cos\tau + 3\cos(\tau - 2\nu)\right]$,

where $\tau = \angle\vec{M}, \hat{P}$, $\nu = \angle\hat{e}, \vec{M}$ and $\vec{M}$ is the Co magnetization. A measurement of the effective spin moment along a photon direction $\hat{P}$ will give the sum between the projection of m_{SPIN} along $\hat{P}$ and the magnetic dipole term, which can be evaluated using (3). In order to calculate m_T we will perform measurements of the effective spin moment in the following three geometries, shown in Fig. 6: (a) Collinear geometry at $\theta = 45^0$, where $\tau = -45^0 + |\nu|$ and $\nu = -|\nu|$, (b) Transverse geometry at $\theta = 45^0$, where $\tau = -45^0 - |\nu|$ and $\nu = |\nu|$, and (c) Collinear geometry at $\theta = 0^0$ and $\tau = \nu = 0^0$. If we apply formula (3) for each of these three geometries, we get the following set of equations:

$$4a)\ \ m_{SPIN}\cos(-45^0 + |\nu|) + \frac{1}{4} m_T^z \left[\cos(-45^0 + |\nu|) + 3\cos(-45^0 + 3|\nu|)\right] = m_{SPIN}^{eff}(H_Z^{\theta=45^0})$$

$$4b)\ \ m_{SPIN}\cos(-45^0 - |\nu|) + \frac{1}{4} m_T^z \left[\cos(-45^0 - |\nu|) + 3\cos(-45^0 - 3|\nu|)\right] = m_{SPIN}^{eff}(H_X^{\theta=45^0})$$

$$4c)\ \ m_{SPIN} + m_T^z = m_{SPIN}^{eff}(H_Z^{\theta=0})$$

The above set of equations can be solved numerically for m_{SPIN}, m_T^z and $|\nu|$, knowing the effective spin values measured in the three geometries. We remark that the above method for calculating m_T^z does not rely on the assumption that the sample is magnetically saturated. After performing the calculations we find that the magnetic dipole term values are only a small fraction (~ 6% or less) of the spin moment at all thicknesses. These dipole term values are close to values reported for Au/Co/Au structures [7,16] and will be neglected in the following analysis.

We plot in Fig.7 (a) the thickness dependence of the spin moment obtained from Eq. 2 with $m_T = 0$. The value of 0.65 μ_B/hole which we obtain for Co(2nm) is close to

previously reported values [16]. We notice a decrease in the spin moment of up to about 50% at the lowest thickness. This cannot be attributed to a reduced Curie temperature of the thinnest layers, as generally observed in thin films [41]. Previously published studies of Co/Cu [42, 43] and Pt/Co/Pt [44] indicate that the Curie temperature of a 0.6nm Co layer is above 400K and suggest that only a small magnetic moment reduction (around 10%) can be induced by the lower Curie temperature of the film. Moreover, the strong PMA of Pt/Co/AlO_x is expected to further stabilize ferromagnetism compared to Co/Cu and Pt/Co/Pt layers. For an underoxidized AlO_x layer it was found that interfacial Co-Al-O bonds predominate, which favors a charge transfer between Al and Co that can reduce the net Co magnetic moment [45]. However it appears more likely that our samples are slightly overoxidized, in which case the low value we obtain for the Co spin moment can be explained by the dilution of Co due to migration of O into the Co layer [23]. This is also in agreement with previous reports that found that the average magnetization of Pt/Co(0.6 nm)/AlO_x trilayers reduces to about 60% of the bulk Co value [25]. Figure 7 b) shows that the orbital moment increases with thickness, up to a value of ~ 0.2 μ_B/atom for Co(2nm), which is larger than values reported for bulk Co orbital moments of ~ 0.15 μ_B/atom [46]. For the number of holes we used n_{3d} = 2.49 [42,43]. The decrease in orbital moment at lower thickness can be partially correlated with the decrease in the spin moment, i.e., to oxidation effects. However, we see that the orbital to spin moment ratio goes up with decreasing thickness [Fig. 7 (c)], which we interpret as an enhancement of the orbital moment at the Co interface. The orbital moment enhancement is discussed in more detail in the next section.

IV. Analysis

A. Noncollinear spin and orbital magnetic moments

By probing the Co layer magnetization along two orthogonal measurement geometries we achieved a vector measurement of the spin and orbital magnetic moments. This is important in order to ascertain the degree of noncollinearity between the two vectors and quantify the orbital magnetization components of this system, which relate to PMA. The Co orbital and spin moment in vector representation are shown in Fig. 8(a) for all four Co thicknesses. To obtain the vector measurements displayed in Fig. 8, three XMCD measurements were performed for each sample thickness (in the geometries shown in Fig. 6), as follows. A measurement in the collinear geometry at $\theta = 45^0$ and one in transverse geometry at $\theta = 45^0$ were necessary in order to get the two cartesian components of m_{ORB}. A third measurement, in collinear geometry at $\theta = 0^0$, was necessary to determine the magnitude and orientation of the spin moment (m_{SPIN} and $\nu_{),}$ as described in the section III.B. We notice that for the Co(0.6 nm) sample the orbital and spin moments are markedly pulled away from the applied field towards the sample normal. This clearly indicates a magnetic anisotropy in the out-of-plane direction. As the Co thickness becomes larger, the orbital and spin moments gradually rotate towards the in-plane direction. We can explain this behavior qualitatively as a competition between the out-of-plane magnetic anisotropy and the shape anisotropy, which favors the in-plane alignment. Moreover, the rather strong dependence of the spin and orbital moment directions on the Co thickness indicates that only a sharp region near the interface is responsible for the anisotropy, dominating any bulk anisotropy contribution.

Figure 8 (b) shows a plot of the angle between the spin and orbital magnetic moments as a function of thickness, which shows that the misalignment between the

two moments becomes largest at the lowest thickness. One interesting issue is the collinearity between m_{SPIN} and m_{ORB} in the presence of a large anisotropy field. It has been shown [15,36] that a large magnetocrystalline anisotropy can render m_{ORB} and m_{SPIN} non-collinear. Our data are consistent with the hypothesis of non-collinearity, since the misalignment we measure between m_{ORB} and m_{SPIN} for Co(0.6 nm) is significant: 6^o +/- 2^o. Note that the sign of the misalignment angle appears to be positive for all thicknesses, which implies that the orbital moment pulls the spin towards the surface normal even in samples with in-plane easy axis, Co(1.5 nm) and Co(2 nm). This agrees with the view that the magnetocrystalline contribution to the magnetic anisotropy is always perpendicular in these systems, but is overcome by the demagnetizing field in the thicker samples.

B. Interfacial orbital magnetic moments

From Fig. 7 (c), we notice that the orbital to spin moment ratio becomes larger with decreasing thickness, which indicates a significantly enhanced orbital contribution at the interface.

The dependence of m_{ORB} and m_{SPIN} on the Co thickness can be further clarified by a simple model which is presented in the following. We assume epitaxial, atomically flat interfaces in which only the interface Co contributes to the magnetic anisotropy. Assuming a uniaxial anisotropy to the lowest order, we can write for the interface Co orbital moment: $m_{ORB}^{\text{int}} = m_{ORB}^{\perp} \cos^2 \gamma + m_{ORB}^{\parallel} \sin^2 \gamma$, where γ is the angle between m_{ORB}^{int} and the sample normal. We will further assume that Co atoms not belonging to the interface Co monolayers (the ¨bulk¨ Co) will not have any contribution to the anisotropy and therefore will possess an orbital moment collinear with and proportional to the spin moment m_{SPIN}. In other words, we postulate no bulk magnetic anisotropy. We also assume that the exchange interaction is strong enough to keep the spin moments aligned

over the entire film thickness, since the Co layer is much thinner than the Co exchange length (~ 7 nm). Under these assumptions, the orbital moment of the full Co layer $m_{ORB}{}^{\gamma}$ is given by the weighted average between the orbital moment of interface Co (anisotropic component) and the orbital moment of bulk Co (isotropic component):

$$(5) \qquad m^{\gamma}_{ORB} = \frac{1}{d}\left[d_1 (m_{ORB}{}^{\perp} \cdot \cos^2 \gamma + m_{ORB}{}^{\parallel} \cdot \sin^2 \gamma) + (d - d_1) \cdot C \cdot m^{\gamma}_{SPIN} \right],$$

where d_1 is the thickness of the interface Co, d is the total thickness of the Co film and C is a constant that gives the ratio between the orbital and the spin magnetic moments in the bulk. Its value for bulk-like hcp Co films is $C \sim 0.1$ [46]. We notice that, as the bulk contribution is dominant in the Co(2nm) layer ($d/d_1 \gg 1$), it is possible to estimate C using the values for the orbital and spin moments in the Co(2nm) film, which gives $m^{\gamma}_{ORB}/ m^{\gamma}_{SPIN} \sim 0.12$. If we further assume that $m_{ORB}{}^{\parallel}$ is equal to the bulk orbital moment, we straightforwardly obtain for the orbital moment anisotropy of the Co(0.6nm) layer, which we define as $m_{ORB}{}^{\perp} - m_{ORB}{}^{\parallel}$, a value of 0.018 μ_B/hole, or 0.045 μ_B/atom, if we substitute for the number of holes $n_{3d} = 2.49$ [47,48]. The rather large value we obtained for the orbital moment anisotropy compared to the measured bulk Co anisotropy (~ 0.009μ_B/atom) [49] justifies our omission of the bulk anisotropy. Note that the interface orbital moment enhancement must have contributions from both Co/AlOx and Co/Pt interfaces, and since it is difficult to separate their respective contributions, we used in the above estimates a value $d_1 = 0.4$ nm (one Co monolayer for each interface). Similar values for interfacial orbital moment enhancement of ~ 0.03 μ_B/atom have been reported in Co/Pt multilayers [10] and ~ 0.1 μ_B/atom in Au/Co/Au structures [16].

We have one remark regarding our assumption that the number of 3d holes is thickness-independent. Charge transfer and hybridization of the *d*-states can be studied

to some degree by integrating the total (white line) XAS intensity normalized to the continuum edge jump. However, this works best at the interface between different elements, whereas small changes of the L_3 and L_2 intensity (related to n_h) are very sensitive to saturation effects in homogenous films with different thickness. We thus assumed the number of holes to be equal to the bulk Co value. This approximation does not affect the main conclusions and trends reported in this paper.

C. Magnetic anisotropy energy

The magnetic anisotropy energy of a thin film has contributions arising from the demagnetizing energy E_{demag} (shape anisotropy) as well as magnetocrystalline anisotropy E_{MCA}. The latter depend on the hybridization of the *d*-electron orbitals at the interface as well as on the degree of epitaxial strain in the magnetic layer. The tight binding model of Bruno [17] relates E_{MCA} of a uniaxial system to the anisotropy of the orbital magnetic moment:

$$E_{MCA} = -\frac{G}{H}\frac{\xi}{4\mu_B}(m_{ORB}^{\perp} - m_{ORB}^{\parallel}), \quad (6)$$

where G/H is a band structure parameter estimated to be 0.2 for Co [16] and ξ is the spin-orbit coupling constant, equal to 0.05 eV. Using the value for $m_{ORB}{}^{\perp} - m_{ORB}{}^{\parallel}$ derived as described in section IV.B we obtain a magnetic anisotropy energy value of 0.11 meV/atom for the Co(0.6nm) layer.

Fully-relativistic band structure calculations performed in the local spin-density approximation [15, 31] have established a connection between the magnetocrystalline anisotropy E_{MCA} and the component of the orbital moment vector L perpendicular to the

spin magnetization, L_{perp}. We calculate for the Co(0.6nm) sample a transverse orbital moment $L_{perp}/n_h \sim -0.063$ (in units of $\hbar = 1$), which according to [15, 31] yields a value $E_{MCA} \sim 0.2$ meV/atom [15], in reasonable agreement with the Bruno model estimation of 0.11 meV.

We will compare the above theoretical estimates of the anisotropy energy with the measured magnetic anisotropy. The experimental anisotropy energy density K_1 can be found by minimizing the total energy E_{tot} of the system at the experimentally measured γ value, where $E_{tot} = E_{MCA} + E_{ext.field} + E_{demag} = -K_1 \cos^2\gamma + 2\pi M^2 \cos^2\gamma - M * H$, where M contains contributions from both spin and orbital moments and $E_{ext.field}$ is the Zeeman energy due to the external magnetic field. We calculate the experimental magnetic anisotropy by setting the effective field $H_{eff} = H_{anis} + H_{ext} + H_{demag}$ parallel to the Co magnetization, where H_{anis}, H_{ext} and H_{demag} are the anisotropy, external and demagnetizing fields respectively. Following this procedure we find for the Co(0.6nm) sample an anisotropy constant $K_1 \sim 1$ MJ/m^3, or ~ 0.07 meV/atom. In this estimate we used the bulk Co density of 8900 kg/m^3 and the measured Co magnetization, which is the sum between the orbital and spin moment contributions. The 0.07 meV/atom anisotropy value obtained this way is likely to be underestimated since it assumes an uniform magnetization over the entire thickness of the Co film, while in reality the Co monolayer nearest to the Co/AlOx interface is at least partially oxidized and therefore carries a substantially lower moment. If we re-derive the experimental anisotropy under the assumption that the top Co monolayer has zero magnetization (and therefore assign a proportionally larger M to the remaining Co monolayers), we get an experimental anisotropy of 0.12 meV/atom.

In spite of the raw assumptions used in the derivation, the experimental value is reasonably close to the value derived using Bruno´s model of 0.11 meV/atom, which enforces the view that spin anisotropy is merely a consequence of orbital moment anisotropy in this class of samples. We want to stress that the two estimates of the magnetic anisotropies described above were independently derived, using the XMCD-measured spin and orbital moment respectively. Our estimates of the magnetic anisotropy are close to values measured on similar Pt/Co(0.6nm)/AlO_x structures of 0.8 MJ/m^3 for the effective anisotropy, which includes the E_{MCA} and E_{demag} terms [23].

D. Relationship between orbital moment anisotropy and Rashba effect

The Rashba effect has been extensively studied in semiconductors [50] and nonmagnetic metal surfaces [51, 52]. Investigations of the Rashba effect in ferromagnets have been limited to the surface of rare-earth thin films probed by angle-resolved photoemission [30, 53]. In a recent study, we have shown that an electric current flowing in the plane of the Pt/Co(0.6nm)/AlO_x trilayer produces an effective magnetic field proportional to the current density and orthogonal to both current and interface potential gradient [27]. Such a field is proportional to $\alpha_R(\mathbf{j}\times\hat{\mathrm{e}})$, consistently with that expected from the combination of the Rashba interaction and *s-d* exchange [28, 54-56]. Here, $\mathbf{j}$ is the current density and α_R is the Rashba constant, a material parameter describing the strength of the interaction. It is known that α_R depends in a rather complicated way on the crystal field potential gradient along $\hat{\mathrm{e}}$, the atomic spin-orbit parameter ξ [50], as well as the orbital character of the interface states [30, 57]. Although the relative influence of these factors might in principle be different, one can easily see that the same parameters determine whether a magnetic material presents PMA or not.

To evidence the relationship between the Rashba effect and PMA, we will discuss the dependency of α_R on the anisotropy of the orbital magnetic moment using arguments derived from simple tight-binding models. Including spin-orbit coupling within nearly-free-electron bands described by anisotropic *p*-states, it was found that the magnitude of the surface Rashba effect is given by:

$$\alpha_R = 6\xi \frac{V_\perp}{V_\parallel}, \quad (7)$$

where $V_\parallel$ and $V_\perp$ represent the hopping parameters between in-plane (x,x; y,y) orbitals and in-plane to out-of-plane (x,z; y,z) orbitals, respectively [58]. A similar relationship can be postulated if the orbital basis set is extended to *s*+*p*+*d* states. From Eq. (7) one can see that the Rashba interaction depends on the atomic spin-orbit parameter of the interfacial states as well as the surface potential gradient, proportional to $V_\perp$. The important point here is that the parameters $V_\parallel$ and $V_\perp$ also determine the in-plane and out-of-plane bandwidth of hybridized states at the interface between two atomic planes. By use of perturbation theory [7,17,59], it can be shown that, omitting constant factors of the order of unity, the in-plane and out-of-plane orbital magnetic moment of nearly two-dimensional magnetic films are approximated by:

$$m_{ORB}^{\perp} \sim \frac{\xi}{V_\parallel}\mu_B, \; m_{ORB}^{\parallel} \sim \frac{\xi}{V_\perp}\mu_B . \quad (8)$$

These relationships reflect the fact that the largest orbital moment is found for wavefunctions that preserve part of their atomic character, i.e., perpendicular to the bonding plane where hybridization is smaller. Although expressions (7) and (8) depend on details of the band structure specific to each system, we can conclude rather generally that the Rashba effect will be stronger in materials that present a large orbital moment anisotropy and PMA, i.e.,

(9) $$\alpha_R \sim \xi \frac{m^{\perp}}{m^{\parallel}}.$$

The XMCD results presented in the previous sections for Pt/Co(0.6nm)/AlO_x together with those reported in Ref. 27 agree with this model. Moreover, Eq. (9) provides clues about the relative strength of the Rashba interaction in different magnetic systems. For instance, based on their strong orbital moment anisotropy [16], we anticipate that Co/Au interfaces with or without an oxide capping should present a remarkable Rashba effect.

V. Conclusions

We performed a vectorial measurement of the Co spin and orbital moment in Pt/Co/AlOx by using the transverse XMCD technique. The absolute values for both spin and orbital magnetic moments were found to increase with Co thickness. However, the orbital-to-spin ratio of the magnetic moments as well as the orbital moment anisotropy are considerably larger in the thinnest Co layers. By using a simple analytical model we estimate an orbital moment anisotropy of 0.045 μ_B/atom for the Co (0.6 nm) sample. We found similar trends for the orbital moment anisotropy and the macroscopic magnetic anisotropy, which confirm that the PMA of Pt/Co/AlO_x structures is related to the anisotropy of the Co interfacial orbital moment. We discussed the occurrence of PMA and Rashba effect in Pt/Co(0.6 nm)/AlO_x , showing that both are related to the anisotropy of the orbital magnetic moment and to a prevalence of the out-of-plane component over the in-plane one.

VI. Acknowledgements

We acknowledge useful discussions with I. M. Miron. Work supported by the European Research Council (StG 203239 NOMAD), Ministerio de Ciencia y Innovación (ERA-Net EUI2008-03884, MAT2010-15659, PTA2008-1108-I), Agència de Gestió d'Ajuts Universitaris i de Recerca (2009 SGR 695), and Nanoaracat. We acknowledge the Diamond Light Source for the provision of beamtime and LMA-INA for access to the electron microscopy facility. J. J. K. thanks the NSF for financial support through Grant No. OISE 0853415.

References

[1] L. Néel, J. Phys. Radium **15**, 225 (1954).

[2] U. Gradmann and J. Müller, Phys. Status Solidi **27**, 313 (1968).

[3] P. F. Garcia, A. D. Meinholdt, and A. Suna, Appl. Phys. Lett. **47**, 178 (1985).

[4] C. Chappert, K. L. Dang, P. Beauvillain, H. Hurdequint, and D. Renard, Phys. Rev. B **34**, 3192 (1986).

[5] B. T. Jonker, K. H. Walker, E. Kisker, G. A. Prinz, and C. Carbone, Phys. Rev. Lett. **57**, 142 (1986).

[6] F. J. A. den Broeder, W. Hoving, and P. J. H. Bloemen, J. Magn. Magn. Mat. **93**, 562 (1991).

[7] J. Stöhr, J. Magn. Magn. Mat. **200**, 470 (1999).

[8] B. Heinrich and J. A. C. Bland, Ultrathin Magnetic Structures (Springer-Verlag, Berlin) (2010); C. A. F. Vaz, J. A. C. Bland, G. Lauhoff, Rep. Prog. Phys. 71, 056501 (2008).

[9] Y. Wu, J. Stöhr, B. D. Hermsmeier, M. G. Samant, and D. Weller, Phys Rev. Lett **69**, 2307 (1992).

[10] N. Nakajima, T Koide, T. Shidara, H. Miyauchi, H. Fukutani, A. Fujimori, K. Iio, T. Katayama, M. Nyvlt, and Y. Suzuky, Phys. Rev. Lett **81**, 5229 (1998).

[11] G. Moulas, A. Lehnert, S. Rusponi, J. Zabloudil, C. Etz, S. Ouazi, M. Etzkorn, P. Bencok, P. Gambardella, P. Weinberger, and H. Brune, Phys. Rev. B **78**, 214424 (2008).

[12] P. Gambardella, S. Rusponi, T. Cren, N. Weiss, and H. Brune, C. R. Physique **6**, 75 (2005).

[13] P. Gambardella, S. Rusponi, M. Veronese, S. S. Dhesi, I. Cabria, R. Zeller, P. H. Dederichs, A. Dallmeyer, C. Grazioli, K. Kern, C. Carbone, and H. Brune, Science **300**, 1130 (2003).

[14] P. Gambardella, A. Dallmeyer, K. Maiti, M. C. Malagoli, W. Eberhardt, K. Kern, and C. Carbone, Nature **416**, 301 (2002).

[15] H. A. Dürr, G. Y. Guo, G. van der Laan, J. Lee, G. Lauhoff, and J. A. C. Bland, Science **277**, 213 (1997).

[16] D. Weller, J. Stöhr, R. Nakajima, A. Carl, M. G. Samant, C. Chappert, R. Megy, P. Beauvillain, P. Veillet, and G. A. Held, Phys. Rev. Lett. **75**, 3752 (1995).

[17] P. Bruno, Phys Rev. B 39, 865 (1989).

[18] G. van der Laan, J. Phys.: Condens. Matter 10, 3239 (1998).

[19] S. Monso, B. Rodmacq, S. Auffret, G. Casali, F. Fettar, B. Gilles, B. Dieny, and P. Boyer, Appl. Phys. Lett **80**, 4157 (2002).

[20] B. Rodmacq, S. Auffret, B. Dieny, S. Monso, and P. Boyer, J. Appl. Phys. **93**, 7513 (2003).

[21] Y. Dahmane, S.Auffret, U. Ebels, B. Rodmacq, and B. Dieny, IEEE Trans. Magn. **44**, 2865 (2008).

[22] L. E. Nistor, B. Rodmacq, S. Auffret, and B. Dieny, Appl. Phys. Lett **94**, 012512 (2009).

[23] B. Rodmacq, A. Manchon, C. Ducruet, S. Auffret, and B. Dieny, Phys. Rev. B **79**, 024423 (2009).

[24] A. Manchon, S. Pizzini, J. Vogel, V. Uhlir, L. Lombard, C. Ducruet, S. Auffret, B. Rodmacq, B. Dieny, M. Hochstrasser, and G. Panaccione, J. Appl. Phys. **103**, 07A912 (2008).

[25] A. Manchon, S. Pizzini, J. Vogel, V. Uhlir, L. Lombard, C. Ducruet, S. Auffret, B. Rodmacq, B. Dieny, M. Hochstrasser, and G. Panaccione, J. Magn. Magn. Mat. **320**, 1889 (2008).

[26] E. Y. Tsymbal and K. D. Belashenko, J. Appl. Phys. **97**, 10C910 (2005).

[27] I. M. Miron, G. Gaudin, S. Auffret, B. Rodmacq, A. Schuhl, S. Pizzini, J. Vogel, and P. Gambardella, Nat. Mater. **9**, 230 (2010).

[28] A. Manchon and S. Zhang, Phys. Rev. B **78**, 212405 (2008).

[29] P. Gambardella and I. M. Miron, Phil. Trans. Royal Soc. A 369, 3175 (2011).[30] O. Krupin, G. Bihlmayer, K. Starke, S. Gorovikov, J. E. Prieto, K. Döbrich, S. Blügel, and G. Kaindl, Phys. Rev. B **71**, 201403(R) (2005).

[31] G. Y. Guo, W. M. Temmerman, and H. Ebert, Physica B **172**, 61 (1992).

[32] Samples studied in reference [27], grown under the same conditions and having the same composition as ours were measured repeatedly for coercivity and Rashba field effects during large time intervals (> 1 year) with very reproducible results.

[33] B. T. Thole, P. Carra, F. Sette, and G. van der Laan, Phys Rev. Lett. **68**, 1943 (1992).

[34] P. Carra, B. T. Thole, M. Altarelli, and X. Wang, Phys Rev. Lett. **70**, 694 (1993).

[35] J. Stöhr and H. König, Phys. Rev. Lett. **75**, 3748 (1995).

[36] G. van der Laan, Phys. Rev. B **57**, 5250 (1998).

[37] H. A. Dürr and G. van der Laan, Phys. Rev. B **54**, R760 (1996).

[38] R. Nakajima, J. Stöhr, and Y. U. Idzerda, Phys. Rev. B **59**, 6421 (1999).

[39] By taking a linear combination of the sum rules, equations (1) and (2), we can easily show that $\int_{L_3}(I_- - I_+)dE \sim (m_{SPIN}+3m_{ORB})$, provided we neglect the dipole contribution m_T which is usually small. Since m_{ORB} is a fixed fraction of m_{SPIN} and because $M_{Co} = m_{SPIN} + m_{ORB}$, we can write $M_{Co} \sim \int_{L_3}(I_- - I_+)dE$. If we further assume that the area of the L_3 edge absorption is proportional to its maximum (peak) absorption, we find $R \sim \int_{L_3}(I_- - I_+)dE \sim M_{Co}$.

[40] A.Manchon, C. Ducruet, L. Lombard, S. Auffret, B. Rodmacq, B. Dieny, S. Pizzini, J. Vogel, V. Uhlir, M. Hochstrasser, and G. Panaccione, J. Appl. Phys **104**, 043914 (2008).

[41] P Poulopoulos and K Baberschke, J. Phys.: Condens. Matter 11, 9495 (1999).

[42] A. Ney, A. P. Poulopoulos, M. Farle, and K. Baberschke, Phys. Rev. B 62, 11336 (2000).

[43] C. M. Schneider, P. Bressler, P. Schuster, and J. Kirschner, PRL 64, 1059 (1990).

[44] P. J. Metaxas, J. P. Jamet, A. Mougin, M. Cornier, J. Ferre, V. Baltz, B. Rodmacq, B. Dieny, and R. L. Stamps, Phys. Rev. Lett. 99, 217208 (2007).

[45] I. I. Oleinik, E. Yu. Tsymbal, and D. G. Pettifor, Phys. Rev. B **62**, 3952 (2000)

[46] C. T. Chen, Y. U. Idzerda, H.-J. Lin, N. V. Smith, G. Meigs, E. Chaban, G. H. Ho, E. Pellegrin, and F. Sette, Phys. Rev. Lett. **75**, 152 (1995)

[47] R. Wu and A. J. Freeman, Phys Rev. Lett **73**, 1994 (1994)

[48] G. Y. Guo, H. Ebert, W. M. Temmerman, and P. J. Durham, Phys Rev. B **50**, 3861 (1994).

[49] R. Pauthenet, J. Appl. Phys. 53, 8187 (1982).

[50] R. Winkler, Spin-orbit coupling effects in two-dimensional electron and hole systems (Springer, Berlin) (2003).

[51] S. LaShell, B. A. McDougall, and E. Jensen, Phys. Rev. Lett. **77**, 3419 (1996).

[52] F. Reinert, G. Nicolay, S. Schmidt, D. Ehm, and S. Hüfner, Phys. Rev. B **63**, 115415 (2001).

[53] O. Krupin, G. Bihlmayer, K. M. Doebrich, J. E. Prieto, K. Starke, S. Gorovikov, S. Bluegel, S. Kevan, and G. Kaindl, New J. Phys. **11**, 013035 (2009).

[54] A. Manchon and S. Zhang, Phys. Rev. B **79**, 094422 (2009).

[55] I. Garate and A. H. MacDonald, Phys. Rev. B **80**, 134403 (2009).

[56] A. Matos-Abiague and R. L. Rodriguez-Suarez, Phys. Rev. B **80**, 094424 (2009).

[57] H. Bentmann, F. Forster, G. Bihlmayer, E. V. Chulkov, L. Moreschini, M. Grioni, F. Reinert, Europhys. Lett., **87,** 37003 (2009).

[58] L. Petersen and P. Hedegård, Surf. Sci. **459**, 49 (2000).

[59] D. S. Wang, R. Wu, and A. J. Freeman, Phys. Rev. B **47**, 14932 (1993).

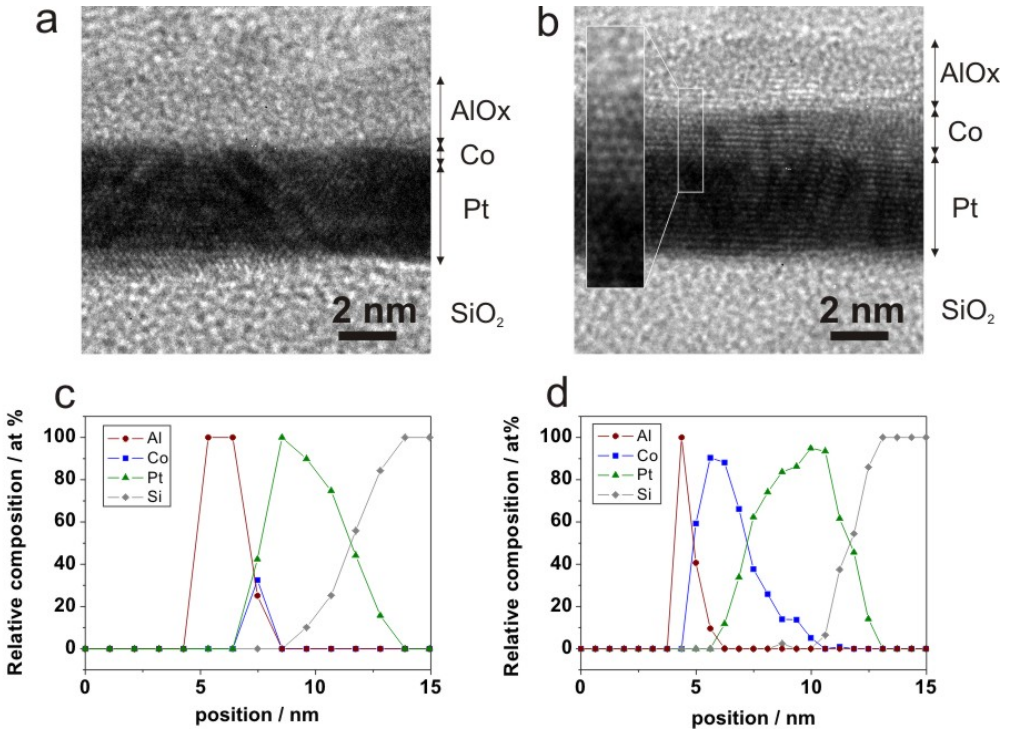

Fig. 1 (color online) HRTEM images of the (a) Pt(3nm)/Co(0.6nm)/AlO_x and (b) Pt(3nm)/Co(2nm)/ AlO_x trilayers. The composition profiles for Al, Co, Pt and Si obtained by EDS-STEM linescans in the same regions are shown in (c) and (d).

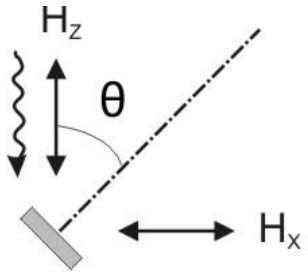

Fig. 2 Diagram of the collinear (H_z) and transverse (H_x) measurement geometries. The sample normal makes an angle θ with the x-ray photon direction.

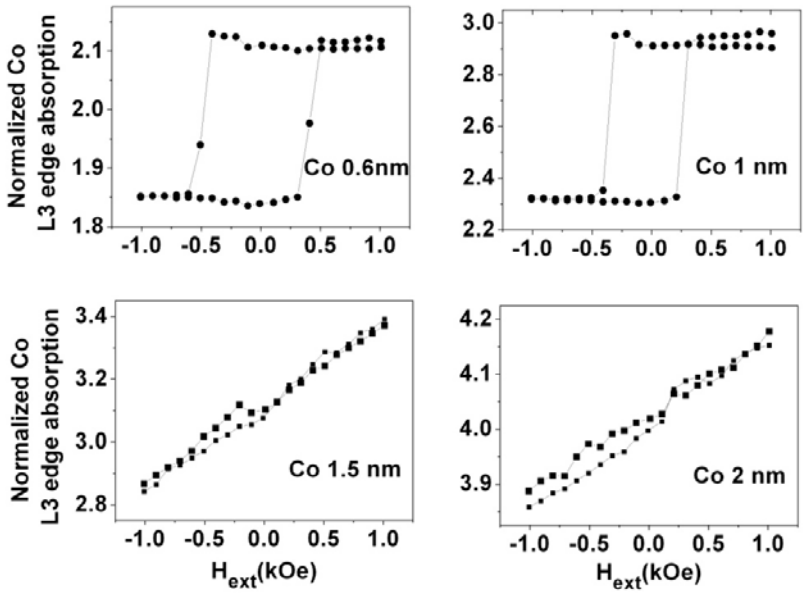

Fig. 3 Perpendicular magnetization curves. The plots show the peak x-ray absorption intensity at the L_3 edge divided by the pre-edge absorption, reflecting changes of the XMCD signal as a function of applied field. All data were taken in the collinear geometry with $\theta=0^{o}$.

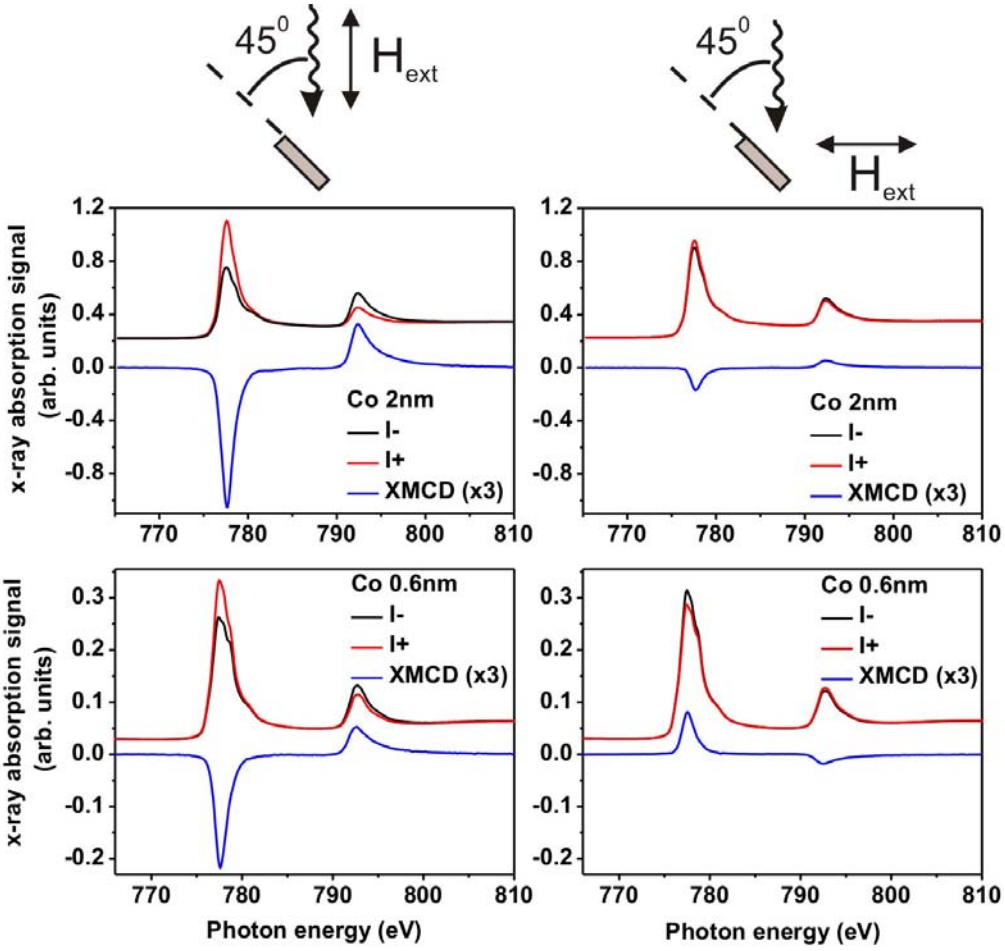

Fig. 4 (color online) XAS and XMCD spectra at the Co $L_{2,3}$ edges for Co (2nm) and Co (0.6nm), taken in collinear (left panels) and transverse (right panels) measurement geometries.

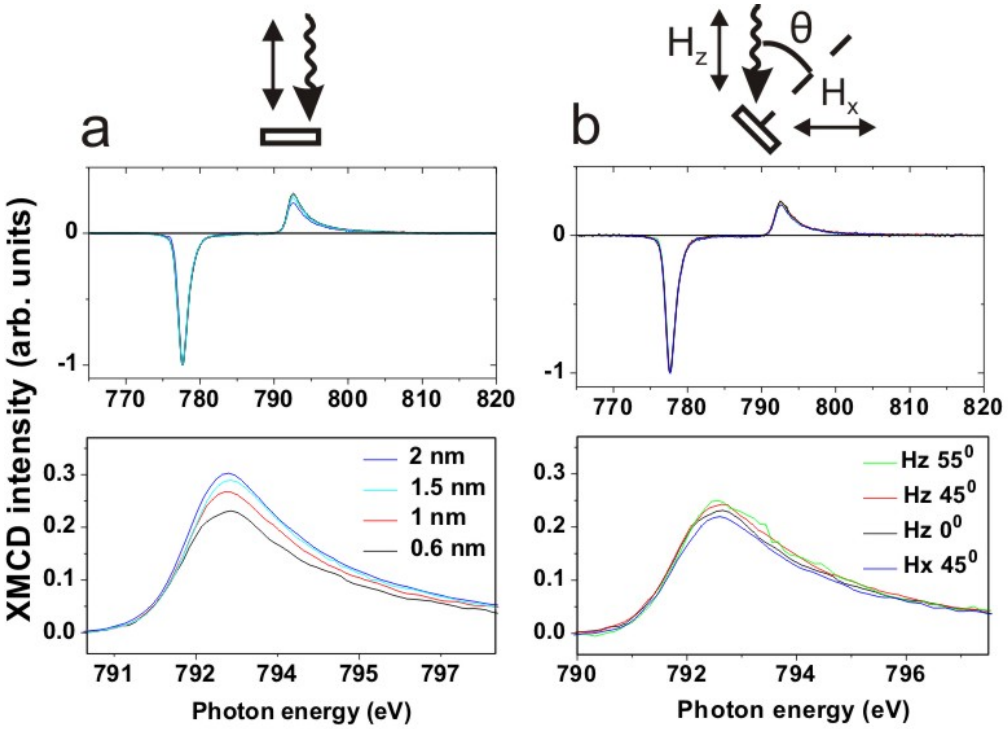

Fig. 5 (color online) Normalized XMCD spectra (a) for different Co thicknesses in the collinear geometry at θ=0º and (b) for Co(0.6nm) in different measurement geometries and sample orientation The L_3 peak was normalized to -1 in all spectra. The measurement geometries in b) are indicated in the schematic drawing and follow the notation in Fig. 2. The angles in the legend are values of θ.

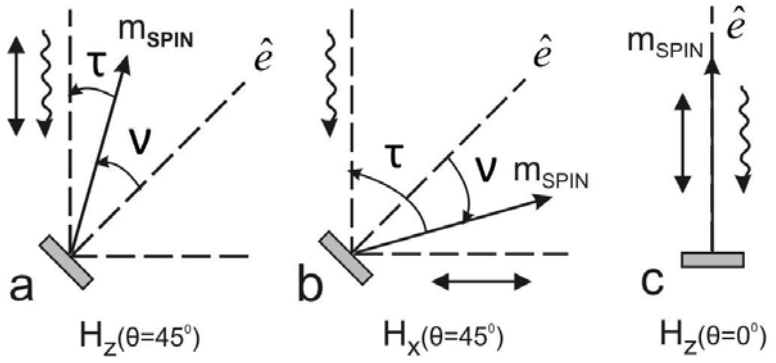

Fig. 6 Diagram of the three measurement geometries used to derive the magnetic dipole term (as discussed in section III.B). τ and ν are angles that relate the spin moment, the sample normal $\hat{e}$ and the x-ray beam direction. The double-arrowed vector shows the direction of the applied field.

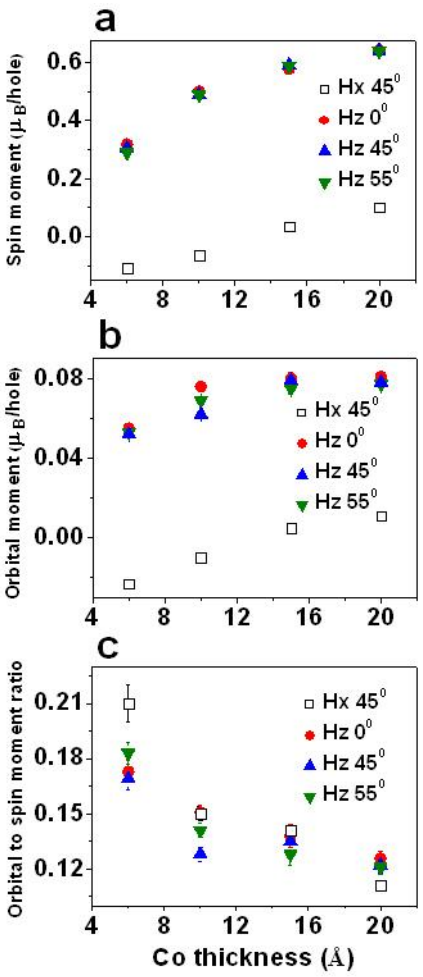

Fig. 7 (color online) Thickness dependence of: a) the spin moment, b) the orbital moment and c) the ratio between orbital moment and spin moment at different measurement geometries. The measurement geometries are indicated in the inset and follow the notation in Fig. 2 The angles are values of θ.

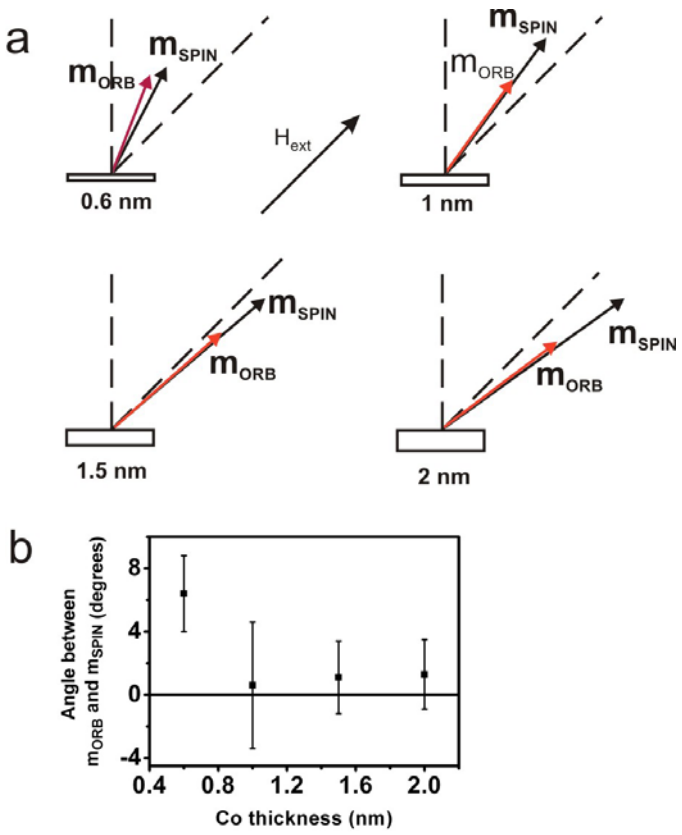

Fig. 8 (color online) a) Vectorial representation of the spin and orbital magnetic moments for four different Co layer thicknesses. An external field H_{ext}=1.95 T is applied at 45^0 with respect to the sample normal (field direction indicated by a dotted line). All orbital and spin moment magnitudes are drawn to scale. b) Misalignment angle between m_{ORB} and m_{SPIN} as a function of Co layer thickness. The misalignment is within the measurement uncertainty at all Co thicknesses except 0.6 nm.